Supporting Information

Lu et al. 10.1073/pnas.1201366109

SI Materials and Methods

Model of the Bistable Mitotic Switch with Multisite Phosphorylation. The present model is based on a previous model of the mitotic switch with distributive, multisite phosphorylation (1). However, we modify some assumptions about the multisite phosphorylation mechanism and how the phosphorylations affect the activity of Wee1 and Cdc25. We also assume that entry into mitosis takes place when the total concentration of Cdc25 reaches a threshold concentration, because Cdc13 levels are not rate-limiting in fission yeast (2). These changes allow the model described below to replicate the different lengths of the phosphorylation site mutants.

We assume that both Cdc25 and Wee1 are phosphorylated at multiple sites by cyclin-dependent kinase 1 (Cdk1) and that phosphorylation results in Cdc25 activation and Wee1 inactivation. The activities of Cdc25 and Wee1 will, therefore, depend on the concentrations of the different phosphoforms and their respective activities.

First, because the length of Cdc25 phosphomutants increases gradually as phosphorylation sites are mutated, we reasoned that the activity should increase gradually with each phosphorylation. The simplest assumption is that phosphorylation leads to a linear increase in activity.

Second, because the data indicate that it is the number of mutated sites that determines length at division and not the identity of these sites, we reasoned that the phosphorylation of Cdc25 follows a disordered phosphorylation mechanism. Our in vitro Cdk1 kinase assay further indicates that Cdc25 phosphorylation is distributive in nature. Third, to achieve ultrasensitivity in the response of Cdc25 to mitosis-promoting factor (MPF; Cdk1-Cdc13), we assume that phosphorylation is cooperative. That is, we assume that the rate of each phosphorylation reaction increases linearly with the number of phosphorylations (the rate of dephosphorylation decreases with the number of phosphorylations). We assume that this mechanism leads to steady-state equations for each phosphoform that closely resemble the equations for an ordered mechanism, which is shown below.

For simplicity, we assume a similar scheme for Wee1 regulation by Cdk1 phosphorylation, although in this case, the activity decreases linearly with the number of phosphorylations. In our model, ultrasensitivity in the responses of Wee1 and Cdc25 to MPF results from the cooperative phosphorylation mechanism (3). In reality, there are probably other sources of ultrasensitivity, such as phosphatase regulation (4) and substrate competition (5). We could also assume more complicated changes in activity to closely fit the length of the phosphorylation site mutants, but this assumption could lead to a much more complicated model and risks overfitting the data.

To describe the model, we derive general equations for the multisite phosphorylation mechanism to calculate the concentration of each phosphoform. We consider a protein X with n possible phosphorylations sites phosphorylated by a kinase k and dephosphorylated by a phosphatase p, where X_i is the form with i phosphorylations (6). For a disordered mechanism, the rates of the reactions change with the number of phosphorylations (6). For the phosphorylation reactions,

$$X_0 \xrightarrow{nk} X_1 \xrightarrow{(n-1)k} X_2 \xrightarrow{(n-2)k} \cdots \xrightarrow{k} X_n,$$

because the number of available sites decreases with each phosphorylation. Similarly, for the dephosphorylation reactions,

$$X_0 \xleftarrow[p]{} X_1 \xleftarrow[2p]{} X_2 \xleftarrow[3p]{} \cdots \xleftarrow[np]{} X_n.$$

If we assume linear positive cooperativity, the phosphorylation rates increase by a factor γ after each phosphorylation site; therefore, combined with the disordered mechanism, they become

$$X_0 \xrightarrow{\gamma nk} X_1 \xrightarrow{\gamma 2(n-1)k} X_2 \xrightarrow{\gamma 3(n-2)k} \cdots \xrightarrow{\gamma nk} X_n.$$

Similarly, the dephosphorylation rates decrease by a factor δ with each phosphorylation, and the rates of the dephosphorylation reactions are

$$X_0 \xleftarrow[\delta np]{} X_1 \xleftarrow[\delta(n-1)2p]{} X_2 \xleftarrow[\delta(n-2)3p]{} \cdots \xleftarrow[\delta np]{} X_n.$$

Written in this way, the factors γ and δ can be incorporated into the kinase and phosphatase activities k and p. Assuming that all of the phosphorylation and dephosphorylation reactions are in equilibrium and that the sum of all of the phosphoforms is X_T, the concentration of each phosphophorm is described by an expression similar to the expression derived for ordered phosphorylation (6), because the factors for the disordered and cooperative mechanisms cancel each other out (Eq. **S1**):

$$X_i = X_T \frac{\left(\frac{k}{p}\right)^i}{\sum_{j=0}^{n}\left(\frac{k}{p}\right)^j}. \qquad [S1]$$

We use this result to calculate the concentrations of each phosphoform of Cdc25 and Wee1. We assume that Cdc25 has a total of n_c Cdk1 phosphorylation sites and that the sum of the concentrations of all of the forms is $Cdc25_T$. To define the activity of Cdc25, we assume that the completely unphosphorylated form has a minimum background activity k'_{25} and that the fully phosphorylated form has a maximal activity k''_{25}. We assume that the activity changes linearly, and therefore, for each phosphoform of Cdc25, the activity is (Eq. **S2**)

$$\phi_{25,i} = k'_{25} + \alpha i, \qquad [S2]$$

where α is the slope of the activity increase given by (Eq. **S3**)

$$\alpha = \frac{k''_{25} - k'_{25}}{n_c}. \qquad [S3]$$

Additionally, we can calculate the total Cdc25 activity, ϕ_{25}, as the sum of the products of the activity of each phosphoform and its concentration for any value of the kinase to phosphatase ratio (Eq. **S4**):

$$\phi_{25} = \phi_{25,0}Cdc25_0 + \phi_{25,1}Cdc25_1 + \phi_{25,2}Cdc25_2 + \cdots + \phi_{25,n_c}Cdc25_{n_c} = \sum_{i=0}^{n_c}\phi_{25,i}Cdc25_i. \qquad [S4]$$

Using the previous result for the concentration of the phosphoforms, the total Cdc25 activity is then (Eq. **S5**)

$$\phi_{25} = Cdc25_T\left(k'_{25} + \alpha\frac{\sum_{i=0}^{n_c} i\left(\frac{k}{p}\right)^i}{\sum_{j=0}^{n_c}\left(\frac{k}{p}\right)^i}\right). \qquad [S5]$$

The summations on the fraction of the above equation can be simplified, because (Eq. **S6**)

$$\sum_{i=0}^{n} ix^i = \frac{x-(n+1)x^{(n+1)}+nx^{n+2}}{(1-x)^2}, \qquad [S6]$$

and the sum of a geometric series is (Eq. **S7**)

$$\sum_{i=0}^{n} x^i = \frac{1-x^{n+1}}{1-x}. \quad \textbf{[S7]}$$

Finally, the equation for the activity of cdc25 becomes (Eq. **S8**)

$$\phi_{25} = Cdc25_T k_{25}, \quad \textbf{[S8]}$$

where (Eq. **S9**)

$$k_{25} = k'_{25} + \alpha \frac{\left(\frac{k}{p}\right) - (n_c+1)\left(\frac{k}{p}\right)^{n_c+1} + n_c\left(\frac{k}{p}\right)^{n_c+2}}{\left(1-\frac{k}{p}\right)\left(1-\left(\frac{k}{p}\right)^{n_c+1}\right)}, \quad \textbf{[S9]}$$

which gives the response of Cdc25 to Cdk1 (Fig. 5*A*). In this case (Eq. **S10**),

$$\frac{k}{p} = \frac{V_{a25} MPF}{V_{i25}}, \quad \textbf{[S10]}$$

where *MPF* is the concentration of active Cdk1-Cdc13 dimers, V_{a25} is a rate constant for phosphorylation of Cdc25 by MPF, and V_{i25} is the rate constant for Cdc25 dephosphorylation by a constant phosphatase activity, part of which corresponds to Clp1.

To model the effect of mutating the Cdk1 phosphorylation sites on Cdc25, we reduce the parameter describing the total number of phosphorylations, n_c. However, the parameter α remains the same, because the activity profile of the different phosphoforms does not change by reducing the number of sites.

For Wee1, we assume that the completely dephosphorylated form has a maximal activity k''_{wee} and that the fully phosphorylated form has a minimum activity k'_{wee}. If Wee1 has n_w possible Cdk1 phosphorylations sites and the concentrations of all of the phosphoforms sum to $Wee1_T$, we derive an equation for the Wee1 activity with respect to MPF (Fig. S5*A*), ϕ_{wee}, similar to the equation for Cdc25 (Eq. **S11**):

$$\phi_{wee} = Wee1_T k_{wee}, \quad \textbf{[S11]}$$

where (Eq. **S12**)

$$k_{wee} = k''_{wee} + \beta \frac{\left(\frac{V_{iwee} MPF}{V_{awee}}\right) - (n_w+1)\left(\frac{V_{iwee} MPF}{V_{awee}}\right)^{n_w+1} + n_w\left(\frac{V_{iwee} MPF}{V_{awee}}\right)^{n_w+2}}{\left(1-\left(\frac{V_{iwee} MPF}{V_{awee}}\right)\right)\left(1-\left(\frac{V_{iwee} MPF}{V_{awee}}\right)^{n_w+1}\right)}. \quad \textbf{[S12]}$$

V_{iwee} is a rate constant for Wee1 phosphorylation by MPF, V_{awee} is the rate constant for Wee1 dephosphorylation by a constant phosphatase, and $\beta = (k'_{wee} - k''_{wee})/n_w$.

To complete the model, we write a differential equation for MPF, which is regulated by Wee1 and Cdc25 (Eq. **S13**):

$$\frac{dMPF}{dt} = k_{25} Cdc25_T (Cyc_T - MPF) - \phi_{wee} MPF, \quad \textbf{[S13]}$$

where Cyc_T, the total amount of cyclin, is the sum of the active and inactive Cdk1-Cdc13 dimers. Assuming that the system is in steady state, for any value of Cyc_T, it is possible to calculate $Cdc25_T$ with respect to *MPF* (Eq. **S14**):

$$Cdc25_T = \frac{\phi_{wee} MPF}{k_{25}(Cyc_T - MPF)}. \quad \textbf{[S14]}$$

To fit our model to the experimental data, we assume that the length of cells at division is proportional to the Cdc25 threshold for MPF activation (that is, the saddle node bifurcations shown in Fig. 5*A*). Because Cdc13 does not seem to be rate-limiting for MPF activation, we assume that, when $Cdc25_T$ reaches the threshold, cyclin levels are already very high. Therefore, a change in their values has little effect on cell size (Fig. S5*D*, two-parameter bifurcation diagram).

For each Cdc25 phosphomutant, we numerically determined the value of the $Cdc25_T$ threshold, θ, and calculated a scaling factor to fit these thresholds obtained from the model to the experimental data. We assume that the cyclin threshold is proportional to length at division (Eq. **S15**),

$$l = \eta\theta, \quad \textbf{[S15]}$$

where l is the length at division, and η is the scaling factor. Therefore, for each mutant, the scaling factor is (Eq. **S16**)

$$\eta = \frac{l}{\theta}. \quad \textbf{[S16]}$$

We use the average of the scaling factors for all of the phosphomutants, η_a, to fit the model to the experimental data for all of the phosphomutants, cell cycle mutants, and variability analysis; therefore, the estimated length at division for each mutant is (Eq. **S17**)

$$l_e = \eta_a \theta. \quad \textbf{[S17]}$$

Table S2 shows the parameter values used for the model, and Table S3 describes the parameters changed to model the cell cycle mutants.

Variation of Cell Size Caused by Variation in Parameter Values. To determine whether elimination of one of two positive feedback loops in the mitotic switch could explain the increased variability in cell size observed in the *cdc25-13A* mutant cells, we decided to look at the effects of noise in parameter values on cell length in our mathematical model. We generated 10,000 random parameter sets for the model of WT and the same number for the model of the *cdc25-13A* mutant, which lacks the Cdc25-MPF positive feedback loop. To add noise to the model parameters, for each parameter in each set, we sampled values from a normal distribution, with mean equal to the parameter value in the deterministic model and an SD of 2.5%. We did this sampling for all parameters except for the number of phosphorylation sites on Wee1 and Cdc25, which are part of model architecture. Parameters-α and -β were recalculated appropriately using the randomly generated values of the minimal and maximal activity of Cdc25 and Wee1. For each random set, we then calculated the $Cdc25_T$ threshold for MPF activation and the estimated length using Eq. **17**, thus obtaining a distribution of length values, which is shown in Fig. 5*B*.

Molecular Biology Techniques. DNA oligonucleotides were from Integrated DNA Technologies. Plasmid constructions were performed with standard molecular biology techniques. Site-directed mutagenesis was carried out using Quikchange Site-Directed or Lightning Multisite-Directed Mutagenesis Kits (Agilent) according to the manufacturer's suggestions. DNA sequencing by GenHunter was used to verify mutations in plasmids and after whole-cell PCR of mutations integrated at the *cdc25* locus.

Strains, Media, and General Yeast Methods. Yeast strains used in this study are listed in Table S4. *nda3-KM311* cells were grown at 32 °C and arrested at 18 °C for 6.5 h. *cdc25* genes were tagged at the 3′-end at their endogenous loci with V5-3x::kan^R or linker-GFP::kan^R cassettes as previously described (7). Transformations were carried out using a lithium acetate method (8). Integrants of *cdc25* mutants and kan^R cassettes were screened by whole-cell

PCR to assure proper genomic placements. GFP tags were also visualized with fluorescent microscopy to ensure expression.

In Vitro Kinase and Cdc25 Activity Assays. For in vitro MBP-Cdc25 kinase assays, 100 ng (1× Cdk1 levels) or varying levels (0.02–10×) of recombinant Cdk1-Cdc13 were used to phosphorylate 1 μg MBP-tagged proteins in kinase buffer (10 μM Tris·HCl, pH 7.4, 10 μM $MgCl_2$, 100 nM DTT) supplemented with 10 μM cold ATP and 5 μCi γ-[^{32}P]ATP. Proteins were incubated for 30 min at 30 °C, and reactions were terminated by the addition of 1:1 SDS sample buffer. Samples were boiled and separated by SDS-PAGE. Coomassie blue or Western blot staining was used to visualize proteins. Autoradiography was used for detection of phosphorylation.

Cdc25 activity assays were performed as previously described (9, 10). Briefly, 5×10^8 cells from *nda3-KM311* prometaphase-blocked samples were lysed in buffer A (300 mM NaCl, 5 mM Disodium EDTA, 10 mM EGTA, 25 mM Mops-NaOH, 60 mM β-glycerol phosphate, 1 mM Na_3VO_4, 1M DTT, 1 mM PMSF). As loading control, 10 μL each lysate were combined with SDS sample buffer, boiled, resolved by SDS-PAGE, and immunobloted with anti-Cdk1 (PSTAIRE) to detect Cdk1. Anti-V5 antibody and protein G Sepharose (GE Life Sciences) were used to collect Cdc25-V5 from the rest of the lysates. Immunocomplexes were washed with buffer C (100 mM NaCl, 5 mM Disodium EDTA, 10 mM EGTA, 25 mM Mops-NaOH, 1 M DTT, 50 mM NaF, 0.1% Nonidet P-40). Beads containing the mitotic forms of Cdc25-V5 were added to protein lysates of *cdc25-22*–blocked cells (6×10^7) lysed in buffer B (100 mM NaCl, 5 mM Disodium EDTA, 10 mM EGTA, 25 mM Mops-NaOH, 60 mM 1 M DTT, 50 mM NaF, 1 mM PMSF) incubated for 15 min at 30 °C and pelleted. Supernatants were moved to a new tube, and beads were washed with buffer D (100 mM NaCl, 15 mM $MgCl_2$, 10 mM EGTA, 25 mM Mops-NaOH, 60 mM β-glycerol phosphate, 1 mM Na_3VO_4, 1 M DTT, 1 mM PMSF). Protein-bound beads were spun down, and wash buffer was added to buffer B supernatants. SDS sample buffer was added to beads, and samples were boiled and separated by SDS-PAGE. Cdc25-V5 was visualized with anti-Cdc25 antibody. For histone H1 kinase assays, Cdk1-Cdc13 was immunoprecipitated from the remaining supernatants using affinity-purified anti-Cdc13 antibody (GJG8) and incubated with 1 mg histone H1 with 10 μM cold ATP and 5 μCi γ-^{32}P ATP as previously described (11). Histone H1 was visualized by Coomassie staining after boiling with SDS sample buffer and SDS-PAGE separation. The relative activity of Cdc25 was estimated using Eq. **S18**,

$$\text{Specific activity} = \frac{(\text{CPM})/[\text{Histone H1}]}{([\text{Cdc25}]/[\text{Cdk1}])}, \qquad \textbf{[S18]}$$

where (CPM) is counts per minute for ^{32}P-labeled histone H1. [Histone H1] is the relative amount of histone H1 visualized by Coomassie stain and quantified with ImageJ software. Final (CPM)/[Histone H1] was calculated for each experimental group after subtraction of CPM in the untagged control. [Cdc25] and [Cdk1] are the relative amounts of Cdc25 and Cdk1 as determined by quantitative immunoblotting on an Odyssey instrument. Protein levels were calculated using ImageJ software.

Microscopy. Cells were grown at 25 °C or 32 °C to midlog phase, and live cell microscopy was performed using an Ultraview LCI spinning disk confocal microscope (PerkinElmer) with 0.6-μm spacing on Z-series optical sections (60× N.A., 1.4 Plan-Apochromat oil immersion object, 488-nm argon ion laser, and 594-nm helium neon laser) or the Olympus IX71 Personal Deltavision microscope (Applied Precision) with 250 W Xenon LED transillumination (60× N.A., 1.56 oil immersion object, and 2.25 μm optical axis integration). Images were processed using Metamorph7.1 (MDS Analytical Technologies) or softWoRx Explorer (Applied Precision) softwares.

Time-lapse microscopy was done on the Personal Deltavision microscope (Applied Precision) using the Onix Microfluidic Perfusion System (CellAsic) platform at 30 °C for 16 h and analyzed using softWoRx software.

Total cellular Cdc25-GFP fluorescence was measured using ImageJ by equalizing background fluorescence between fields and selectively boxing two areas: (box1) is an area including the cell, and (box2) is an area including both the cell and its surrounding background. Total fluorescence for the cell was obtained by subtracting total fluorescence of (box2) from (box1).

2D Tryptic Peptide Mapping. MBP-Cdc25 or MBP-Cdc25 S143A was purified and subjected to in vitro Cdk1 kinase assay as described (11). ^{32}P-labeled proteins were mixed with SDS sample buffer and boiled before separation by 8% SDS-PAGE; the proteins were then transferred to PVDF membranes. Labeled proteins on PVDF membranes were pretreated with methanol for 30 s and incubated for 30 min at 37 °C in 50 mM ammonium bicarbonate in 0.1% Tween20. Membranes were washed in 1 mL 50 mM ammonium bicarbonate and treated two times with 10 μg trypsin in 50 mM ammonium bicarbonate for 3 h at 37 °C to separate phosphopeptides from membrane. Phosphopeptides were lyophilized and separated on thin layer liquid chromatography plates in two dimensions (electrophoresis at pH 1.9 and chromatography) as previously detailed (12).

MS Sample Preparation. Purified Cdc25 was trichloroacetic acid-precipitated and resuspended in 8 M Urea in 100 mM Tris, pH 8.5. Protein was reduced with 100 mM Tris (2-carboxyethyl) phosphine hydrochloride (Thermo Scientific) and alkylated with 100 mM iodoacetamide (Sigma). After diluting the sample to 2 M urea, the sample was digested overnight with 0.4 μg/μL trypsin or chymotrypsin at 37 °C.

Peptides were loaded onto a diphasic MudPIT column on a pressure loader, separated on a 10-cm, 3-μm C18 column using a 12-point MudPIT salt gradient (13), and analyzed with an LTQ mass spectrometer (Thermo Scientific). Agilent HPLC was used in line with the FAMOS autosampler for 5-μL ammonium acetate injections. Each peptide elution was separated using a 0–90% acetonitrile gradient. Peptide ions were acquired in positive mode with full precursor MS scan ranging from 400 to 2,000 *m/z*, which was followed by fragmentation of the 10 most abundant precursors and their natural loss ions of 98, 49, or 33 *m/z* under collision-induced dissociation, isolation width of 2.0 for the parent ion, and collision energy of 35 V. The instrument acquired at least two spectra per eluting species under dynamic exclusion, with repeat duration and exclusion duration of 1.5 times the chromatographic peak width at the base and an exclusion list of 150 ions.

MS Data Analysis. Spectra conversion and searches were performed using Ma ZQ (Vanderbilt University, 2011). Briefly, MS2 spectra were extracted from Thermo RAW files and converted to DTA files using Scansifter v2.1.25 software. Spectra with less than 20 peaks were excluded from our analysis. Cdc25 peptides were searched against the Sanger Institute *Schizosaccharomyces pombe* protein database (http://old.genedb.org/genedb/pombe/). Database sequences along with contaminant sequences (keratin and IgG isotopes) were reversed and concatenated (14). Searches were performed with the Sequest algorithm (TurboSequest v.27 rev12) on a high-performance computing cluster allowing for carbamidomethylation, oxidation of the methionine, phosphorylation of serine, threonine, and tyrosine, and acylation of the N terminus. Peptide mass tolerance was set to 2.5 *m/z*. The DTA files were searched, with trypsin and chymotrypsin as chosen endoproteases, which allowed 10 modifications per peptide and

a maximum of two missed cleavages. Cdc25 peptides were visualized and validated using Scaffold 3 and Scaffold PTM software (Proteome Software), with the following identification parameters: minimum of 90% probability for correct protein identification, minimum of two peptides per protein, and minimum of 95% peptide match probability.

1. Domingo-Sananes MR, Novak B (2010) Different effects of redundant feedback loops on a bistable switch. *Chaos* 20:045120.
2. Bueno A, Russell P (1993) Two fission yeast B-type cyclins, cig2 and Cdc13, have different functions in mitosis. *Mol Cell Biol* 13:2286–2297.
3. Trunnell NB, Poon AC, Kim SY, Ferrell JE, Jr. (2011) Ultrasensitivity in the Regulation of Cdc25C by Cdk1. *Mol Cell* 41:263–274.
4. Novak B, Kapuy O, Domingo-Sananes MR, Tyson JJ (2010) Regulated protein kinases and phosphatases in cell cycle decisions. *Curr Opin Cell Biol* 22:801–808.
5. Kim SY, Ferrell JEJ, Jr. (2007) Substrate competition as a source of ultrasensitivity in the inactivation of Wee1. *Cell* 128:1133–1145.
6. Kapuy O, Barik D, Sananes MR, Tyson JJ, Novák B (2009) Bistability by multiple phosphorylation of regulatory proteins. *Prog Biophys Mol Biol* 100:47–56.
7. Bähler J, et al. (1998) Heterologous modules for efficient and versatile PCR-based gene targeting in *Schizosaccharomyces pombe*. *Yeast* 14:943–951.
8. Keeney JB, Boeke JD (1994) Efficient targeted integration at leu1-32 and ura4-294 in *Schizosaccharomyces pombe*. *Genetics* 136:849–856.
9. Kovelman R, Russell P (1996) Stockpiling of Cdc25 during a DNA replication checkpoint arrest in *Schizosaccharomyces pombe*. *Mol Cell Biol* 16:86–93.
10. Wolfe BA, Gould KL (2004) Fission yeast Clp1p phosphatase affects G2/M transition and mitotic exit through Cdc25p inactivation. *EMBO J* 23:919–929.
11. Gould KL, Moreno S, Owen DJ, Sazer S, Nurse P (1991) Phosphorylation at Thr167 is required for *Schizosaccharomyces pombe* p34cdc2 function. *EMBO J* 10: 3297–3309.
12. Boyle WJ, van der Geer P, Hunter T (1991) Phosphopeptide mapping and phosphoamino acid analysis by two-dimensional separation on thin-layer cellulose plates. *Methods Enzymol* 201:110–149.
13. McDonald WH, Yates JR, 3rd (2002) Shotgun proteomics and biomarker discovery. *Dis Markers* 18:99–105.
14. Kouranti I, et al. (2010) A global census of fission yeast deubiquitinating enzyme localization and interaction networks reveals distinct compartmentalization profiles and overlapping functions in endocytosis and polarity. *PLoS Biol* 8: e1000471.

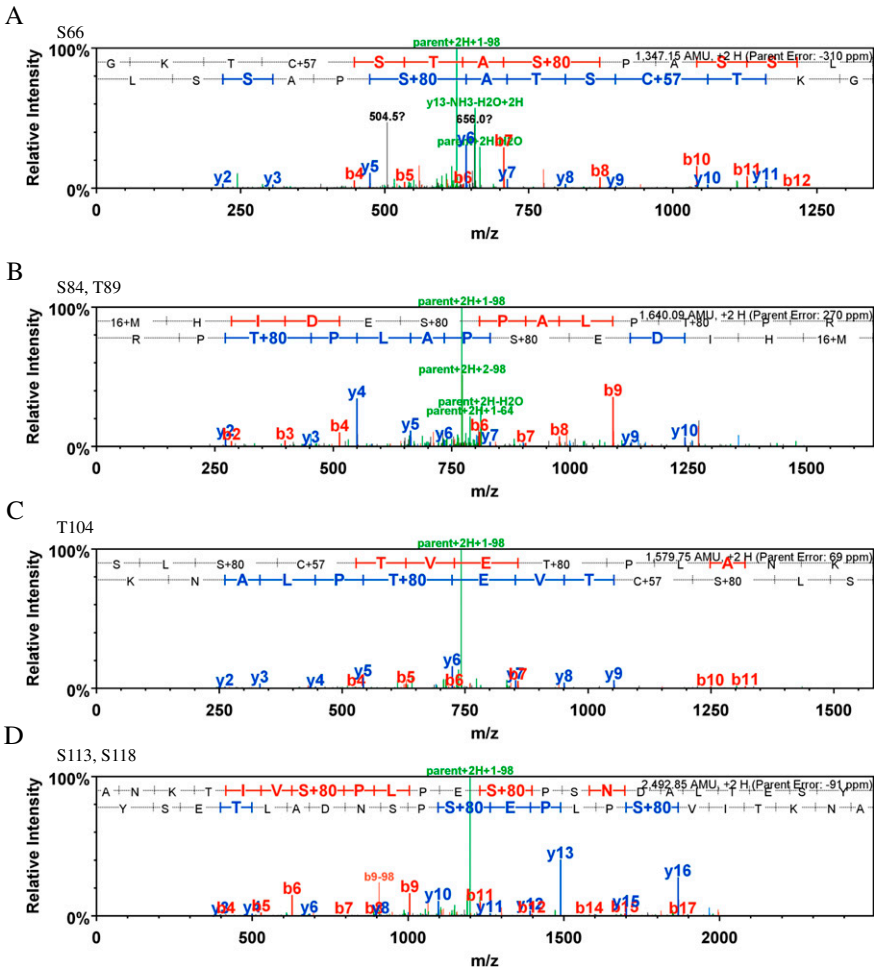

Fig. S1. (Continued)

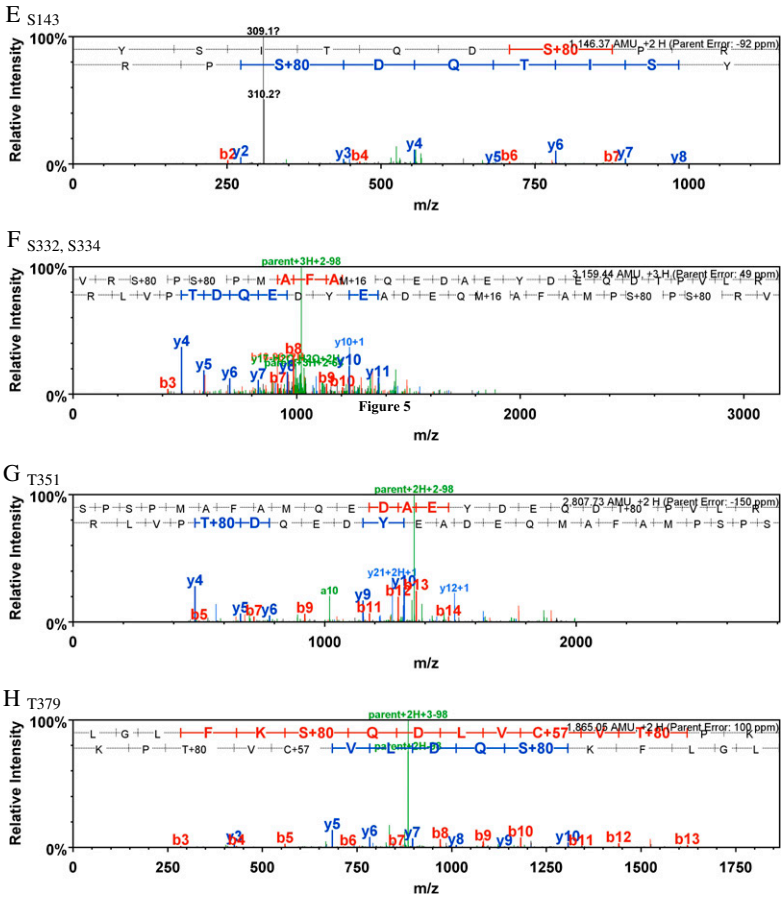

Fig. S1. Representative MS2 spectra of each phosphopeptide listed in Table S1. (*A*–*H*) The peptide sequence ladder depicts identified Y and B ions (blue and red, respectively) of the peptide. Green peaks describe mass to ratio charge of parent ions before fragmentation. Black peaks describe unidentified ions.

A

strain	Mean length (μm)	Variance (μm^2)	Range (μm)	strain	Mean length (μm)	Variance (μm^2)	Range (μm)
no tag	14.3	0.7	12.8 - 16.4				
cdc25-V5	14.2	0.9	12.4-16.9	*cdc25-13A-V5*	20.7	4.8	16.8-28.4
cdc2-L7 cdc25-V5	15.2	1.2	12.9-17.8	*cdc2-L7 cdc25-13A-V5*	25.5	18.7	19.5-35.5
clp1Δ cdc25-V5	11.6	0.8	8.6-14.8	*clp1Δ cdc25-13A-V5*	20.9	5.8	16.7-18.23
cdc2-33 cdc25-V5	14.9	0.7	12.1-17.5	*cdc2-33 cdc25-13A-V5*	26.9	22.9	18.5-39.9
weeΔ cdc25-V5	8.5	2.7	5.8-14.9	*wee1Δ cdc25-13A-V5*	18.0	15.7	5.8-23.7
cdr1Δ cdc25-V5	17.3	1.3	14.6-19.8	*cdr1Δ cdc25-13A-V5*	30.8	34.1	18.6-42.7
cdr2Δ cdc25-V5	18.4	1.3	16.3-22.0	*cdr2Δ cdc25-13A-V5*	35.8	35.7	25.2-49.4
cdc13-117 cdc25-V5	17.2	2.3	15.0-22.6	*cdc13-117 cdc25-13-V5*	24.9	11.2	26.8-31.3

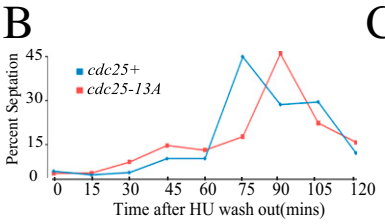

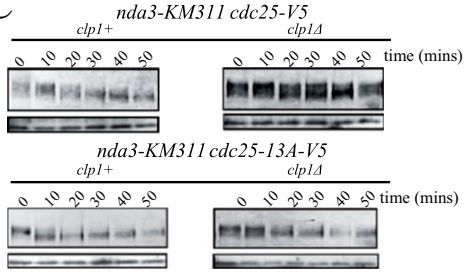

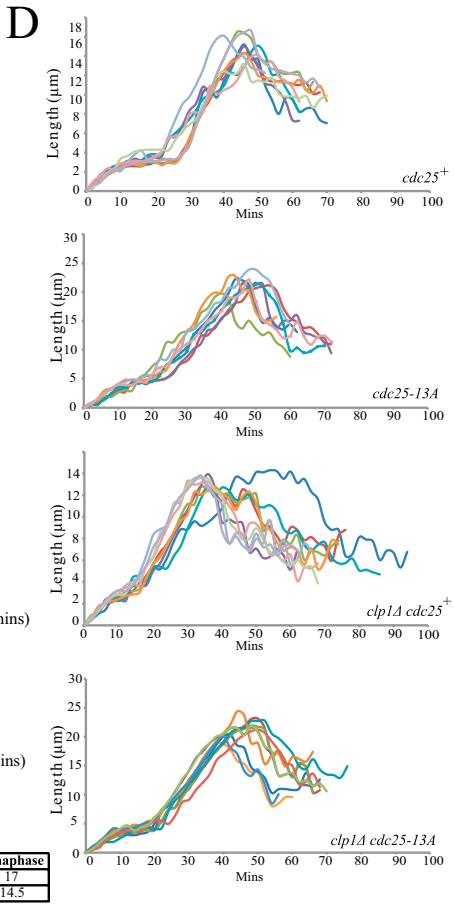

E

length	5.5-7.5	7.5-9.5	9.5-11.5	11.5-13.5	13.5-15.5	15.5-17.5	17.5-19.5	19.5-21.5	prometaphase	anaphase
cdc25+	6.7	4.1	6.7	5.4	10.4	8.5			8.5	17
cdc25-13A		5.4	6.2	6.8	8.1	6.5	15.3	14.7	16.6	14.5

Fig. S2. Cdc25 phosphorylation by Cdk1 mediates timely mitotic entrance and accurate mitotic events. (*A*) Septation lengths of the indicated strains; >100 cells of each strain were measured. Mean length, variance, and range of each strain were calculated and displayed. (*B*) Indicated strains were blocked in S phase using hydroxyurea, and cells were visualized by light microscopy. Cells were released by washing out hydroxyurea and collected at the indicated times. Percent septation was calculated (100 cells per time point). (*C*) Cdc25-V5 was immunoprecipitated with anti-V5 antibody from the indicated strains collected from an *nda3-KM311* block and release at the indicated times. Cdc25-V5 was visualized with anti-Cdc25 antibody (*Upper*). Cdk1 levels in lysates used for immunoprecipitates are visualized with PSTAIRE antibody (*Lower*). (*D*) Indicated strains were grown in yeast extract media. The distances between spindle pole bodies for 10 cells per strain were measured from the beginning of mitosis until the time of septation in 2-min intervals. (*E*) SD for Cdc25-GFP or Cdc25-13A-GFP fluorescence level data for indicated cell lengths.

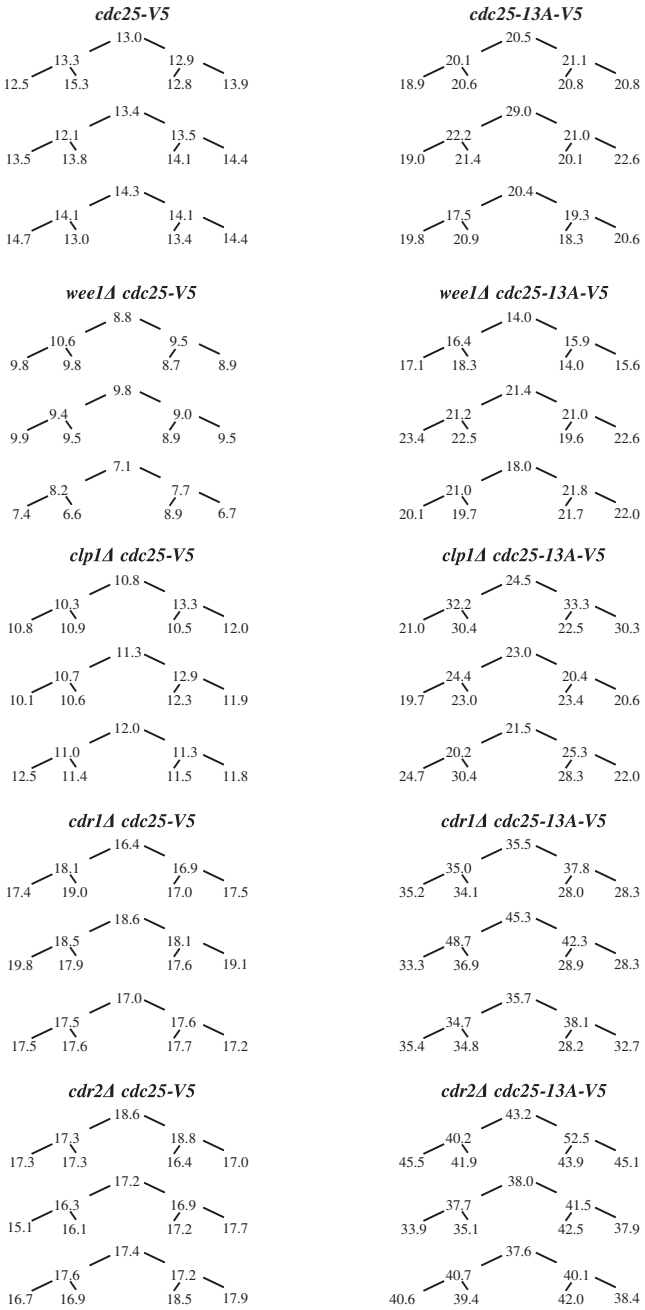

Fig. S3. Representative measurements for cell lengths between generations. For each indicated strain, three separate family trees showing cell lengths (in micrometers) for three generations are shown.

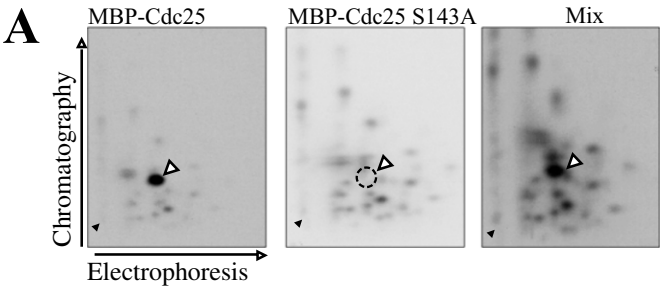

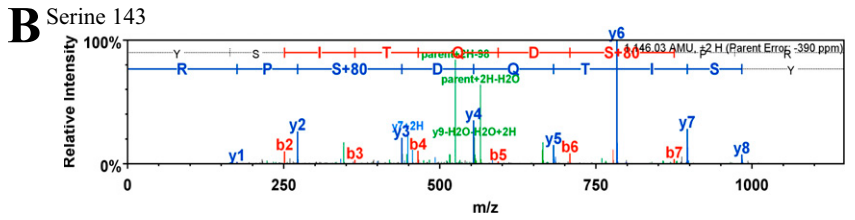

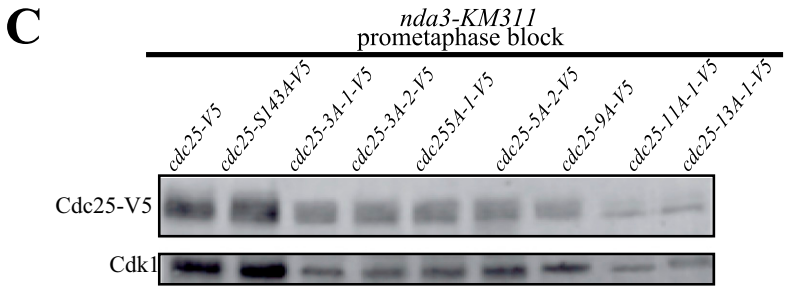

D

S/TP sites	*cdc25+*	*S143A*	*3A-1*	*3A-2*	*5A-1*	*5A-2*	*7A*	*9A*	*11A-1*	*11A-2*	*11A-3*	*13A*
S3								X	X	X		X
S66			X		X		X	X	X	X	X	X
S84						X	X	X	X		X	X
T89									X	X	X	X
T104				X	X		X	X	X	X	X	X
S113						X			X	X	X	X
S118						X	X	X	X	X	X	X
S143		X	X		X		X	X	X	X	X	X
S308						X			X	X	X	X
S332			X	X	X		X	X				X
S334						X		X		X	X	X
T351				X	X		X	X	X	X	X	X
T379									X	X	X	X
mean length (μm)	14.2	14.6	15.1	15.4	15.6	15.5	15.9	17.0	19.1	19.3	19.3	20.1
SEM (μm)	0.1	0.1	0.1	0.2	0.2	0.2	0.1	0.1	0.1	0.1	0.1	0.1

Fig. S4. Removal of Cdk1 phosphosites on Cdc25 additively delays mitosis. (*A*) 2D tryptic peptide maps of MBP-Cdc25 or MBP-Cdc25 S143A, or a mix of the two proteins after in vitro kinase assay with Cdk1. Open triangles indicate location of phosphorylated S143. The dotted circle denotes the position of the missing phosphopeptide when S143 was mutated to alanine. Closed triangles indicate map origins. (*B*) Representative MS2 spectra of the S143-containing phosphopeptide. The peptide sequence ladder depicts identified Y and B ions (blue and red, respectively) of the peptide. Green peaks describe mass to charge ratio of parent ions before fragmentation. Black peaks describe unidentified ions. (*C*) Cdc25-V5 was immunoprecipitated with anti-V5 antibody from the indicated strains arrested in prometaphase and visualized with anti-cdc25 antibody (*Upper*). Cdk1 levels from lysates used for immunoprecipitates are visualized with PSTAIRE antibody (*Lower*). (*D*) The composition of each Cdc25 phosphomutant is diagrammed with mean length and SEM provided.

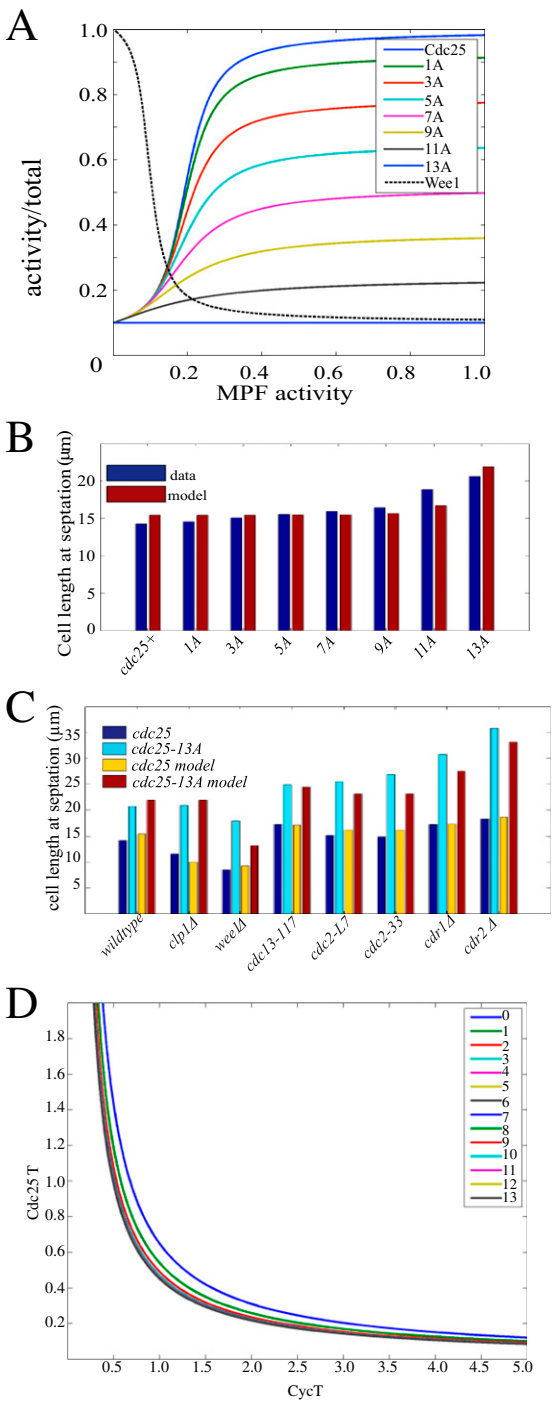

Fig. S5. Mathematical representation of mitotic entrance. (*A*) Cdc25 or Wee1 activity as a function of MPF activity. (*B* and *C*) Experimentally and mathematically predicted values of cell lengths at septation for indicated strains. (*D*) Two-parameter bifurcation diagram of the model for the MPF activation threshold. Observe that the cyclin (Cdc13) level is not rate-limiting in the lower right corner of the diagram and that MPF activation depends on Cdc25 level only.

Table S1. List of confirmed Cdc25 (S/T)P phosphopeptides

Phosphorylation site	Peptide sequence	Localization probability (%)	Delta mass (Da)
S66	GKTCSTA<u>S</u>PASSL	100	1.56
S84	MHIDE<u>S</u>PALP<u>T</u>PR	100	1.44
T89	MKIDE<u>S</u>PALP<u>T</u>PR	100	1.44
T104	SL<u>S</u>CTVE<u>T</u>PLANK	100	1.58
S113	ANKTIV<u>S</u>PLPE<u>S</u>PSNDALTESY	100	0.77
S118	ANKTIV<u>S</u>PLPE<u>S</u>PSNDALTESY	100	0.77
S143	YSITQD<u>S</u>PR	100	1.02
S332	VR<u>S</u>P<u>S</u>PMAFAMQEDAEYDEQDTPVLR	100	1.29
S334	VR<u>S</u>P<u>S</u>PMAFAMQEDAEYDEQDTPVLR	100	1.29
T351	SP<u>S</u>PMAFAMQEDAEYDEQD<u>T</u>PVLR	100	0.612
T379	LGLFK<u>S</u>QDLVC<u>T</u>PK	100	1.37

Phosphorylation site localization probability is derived from SEQUEST and Scaffold PTM algorithms, which consider the number of possible modification sites and intensity of site-specific ions. Delta mass (Daltons) describes the error around the parent ion of the peptide of interest.

Table S2. Parameter values for the model

Parameter	Value
V_{a25}	1
V_{i25}	0.2
V_{awee}	0.2
V_{iwee}	2
n_c	13 (WT)
n_w	11
k'_{25}	0.1
k''_{25}	1
α	0.0692
k'_{wee}	0.1
k''_{wee}	1
β	−0.0818
$Wee1_T$	1
Cyc_T	5

Table S3. Parameter changes for cell cycle mutants

Parameter change	Comment
clp1Δ	
$V_{i25} = 0.1$	Reduce phosphatase on Cdc25 to one-half of the WT
wee1Δ	
$Wee1_T = 0.6$	Reduce Wee1 levels; some activity remains that corresponds to Mik1
cdc13-117	
$V_{a25} = \xi V_{a25,wt}$	Reduce MPF activity on Wee1 and Cdc25 by a factor ξ
$V_{iwee} = \xi V_{iwee,wt}$	Reduce MPF activity on Wee1 and Cdc25 by a factor ξ
$\xi = 0.9$	Reduce MPF activity on Wee1 and Cdc25 by a factor ξ
cdc2-L7	
$V_{a25} = \xi V_{a25,wt}$	Reduce MPF activity on Wee1 and Cdc25 by a factor ξ
$V_{iwee} = \xi V_{iwee,wt}$	Reduce MPF activity on Wee1 and Cdc25 by a factor ξ
$\xi = 0.95$	Reduce MPF activity on Wee1 and Cdc25 by a factor ξ
cdc2-33	
$V_{a25} = \xi V_{a25,wt}$	Reduce MPF activity on Wee1 and Cdc25 by a factor ξ
$V_{iwee} = \xi V_{iwee,wt}$	Reduce MPF activity on Wee1 and Cdc25 by a factor ξ
$\xi = 0.95$	Reduce MPF activity on Wee1 and Cdc25 by a factor ξ
cdr1Δ	
$V_{awee} = 0.25$	Increase phosphatase activity on Wee1
cdr2Δ	
$V_{awee} = 0.3$	Increase phosphatase activity on Wee1

Table S4. Yeast strains used in this study

Strain	Genotype	Reference
Fig. 1		
KGY10328	*h⁻ nda3-KM311 cdc25-V5::kan^R*	This study
KGY10329	*h⁻ nda3-KM311 cdc25-13A-V5::kan^R*	This study
KGY9135	*h⁺ cdc25-13A ura4-D18 leu1-32*	This study
KGY246	*h⁻ ade6-M210 leu1-32 ura4-D18*	Lab stock
KGY11010	*h⁻ nda3-KM311 clp1::ura4⁺ cdc25-13A-V5::kan^R ade6-216 ura4-D18*	This study
Fig. 2		
KGY246	*h⁻ ade6-M210 leu1-32 ura4-D18*	Lab stock
KGY10327	*h⁺ cdc25-V5::kan^R*	This study
KGY10326	*h⁺ cdc25-13A-V5::kan^R ura4-D18 ade6-216 leu1-32*	This study
KGY12201	*h⁻ clp1::ura4⁺ cdc25-V5::kan^R ura4-D18 ade6-216 leu1-32*	This study
KGY11948	*h⁻ clp1::ura4⁺ cdc25-13A-V5::kan^R ura4-D18*	This study
KGY12202	*h⁻ wee1::ura4⁺ cdc25-V5::kan^R ura4-D18 leu1-32*	This study
KGY11683	*h^{90} wee1::ura4⁺ cdc25-13A-V5::kan^R leu1-32 ura4-D18*	This study
KGY11844	*h⁻ cdc13-117 cdc25-V5::kan^R*	This study
KGY11845	*h⁻ cdc13-117 cdc25-13A-V5::kan^R ura4-D18*	This study
KGY11846	*h⁻ cdr2::ura4⁺ cdc25-V5::kan^R ura4-D18*	This study
KGY11847	*h⁻ cdr2::ura4⁺ cdc25-13A-V5::kan^R leu1-32 ura4-D18*	This study
KGY11848	*h⁻ cdc2-L7 cdc25-V5::kan^R*	This study
KGY11849	*h⁺ cdc2-L7 cdc25-13A-V5::kan^R leu1-32*	This study
KGY11686	*h⁺ cdc2-33 cdc25-13A-V5::kan^R ade6-216 leu1-32*	This study
KGY11687	*h^{90} cdc2-33 cdc25-V5::kan^R*	This study
KGY12200	*h⁻ cdr1::ura4⁺ cdc25-V5::kan^R ura4-D18 ade6-216 leu1-32*	This study
KGY12022	*h⁺ cdr1::ura4⁺ cdc25-13A-V5::kan^R ura4-D18 ade6-216 leu1-32*	This study
KGY10264	*h⁺ sid4-RFP::kan^R cdc25-linkerGFP::kan^R ade6-M210 leu1-32 ura4-D18*	This study
KGY10280	*h⁺ sid4-RFP::kan^R cdc25-13A-linkerGFP::kan^R leu1-32 ura4-D18 ade6-216*	This study
Fig. 3		
KGY10264	*h⁺ sid4-RFP::kan^R cdc25-linkerGFP::kan^R ade6-M210 leu1-32 ura4-D18*	This study
KGY10280	*h⁺ sid4-RFP::kan^R cdc25-13A-linkerGFP::kan^R leu1-32 ura4-D18 ade6-216*	This study
KGY42	*h⁻ cdc25-22 ura4-D18 leu1-32*	Lab stock
KGY10328	*h⁻ nda3-KM311 cdc25-V5::kan^R*	This study
KGY10329	*h⁻ nda3-KM311 cdc25-13A-V5::kan^R*	This study
KGY3612	*h⁻ nda3-KM311 ura4-D18 leu1-32*	Lab stock
Fig. 4		
KGY11695	*h⁺ cdc25-5A-1 ade6-216 leu1-32*	This study
KGY11796	*h^{90} cdc25-3A-1 (66A,143A,332A) ura4-D18 leu1-32 ade6-216*	This study
KGY11955	*h⁺ cdc25-3A-2 (104A,332A,351A) ura4-D18 leu1-32*	This study
KGY12615	*h⁺ cdc25-5A-2 ura4-D18 leu1-32 ade6-216*	This study
KGY10715	*h⁺ cdc25-S143A ura4-D18 ade6-M210 leu1-32*	This study
KGY11946	*h⁺ cdc25-11A ura4-D18 leu1-32 ade6-216*	This study
KGY11947	*h^{90} cdc25-7A ade6-216 leu1-32*	This study
KGY11949	*h⁺ cdc25-9A ura4-D18 leu1-32 ade6-M210*	This study
KGY246	*h⁻ ade6-M210 leu1-32 ura4-D18*	Lab stock
KGY9135	*h⁺ cdc25-13A ura4-D18 leu1-32*	This study
Fig. 6		
KGY10328	*h⁻ nda3-KM311 cdc25-V5::kan^R*	This study
KGY10329	*h⁻ nda3-KM311 cdc25-13A-V5::kan^R*	This study
KGY10264	*h⁺ sid4-RFP::kan^R cdc25-linkerGFP::kan^R ade6-M210 leu1-32 ura4-D18*	This study
KGY10280	*h⁺ sid4-RFP::kan^R cdc25-13A-linkerGFP::kan^R leu1-32 ura4-D18 ade6-216*	This study
KGY12023	*h⁺ clp1::ura4⁺ sid4-RFP::kan^R cdc25-13A-linkerGFP::kan^R ura4-D18 ade6-M210 leu1-32*	This study
KGY12072	*h⁻ clp1::ura4⁺ sid4-RFP::kan^R cdc25-linkerGFP::kan^R ura4-D18*	This study

Table S5. Oligonucleotides used for mutagenesis

Oligonucleotide name	Oligonucleotide sequence
cdc25-S3A	5′-AACTAAAATGGATGCTCCGCTTTCTTCAC-3′
cdc25-S3A GC	5′-GTGAAGAAAGCGGAGCATCCATTTTAGTT-3′
cdc25-S66A	5′-TTGTTCGACAGCTGCTCCTGCATCTTCCTT-3′
cdc25-S66A GC	5′-AAGGAAGATGCAGGAGCAGCTGTCGAACAA-3′
cdc25-S84T89A	5′-GCATATCGATGAAGCCCCTGCCTTACCGGCGCCTCGTCGTACGCT-3′
cdc25-S84T89A GC	5′-AGCGTACGACGAGGCGCCGGTAAGGCAGGGGCTTCATCGATATGC-3′
cdc25-S84A	5′-TGCATATCGATGAAGCTCCTGCCTTACCGACTCC-3′
cdc25-S84A GC	5′-GGAGTCGGTAAGGCAGGAGCTTCATCGATATGCA-3′
cdc25-T89A	5′-GCGTACGCCGCGGAGCCGGTAAGGCAGGGCTTTCATCG-3′
cdc25-T89A GC	5′-CGATGAAAGCCCTGCCTTACCGGCTCCGCGGCGTACGC-3′
cdc25-T104S113S118A	5′-CTTTCTTGTACTGTAGAAGCCCCTCTCGCTAACAAGACTATTGTTGCACCTCTCCCCGAGGCACCCTCGAATGACGC-3′
cdc25-T104S113S118A GC	5′-GCGTCATTCGAGGGTGCCTCGGGGAGAGGTGCAACAATAGTCTTGTTAGCGAGAGGGGCTTCTACAGTACAAGAAAG-3′
cdc25-T104A	5′-TCTACTGTAGAAGCTCCTCTCGCTAAC-3′
cdc25-T104A GC	5′-GTTAGCGAGAGGAGCTTCTACAGTAGA-3′
cdc25-S113S118A	5′-AAGACTATTGTTGCTCCTCTCCCGGAGGCTCCCTCGAATGACG-3′
cdc25-S113S118A GC	5′-CGTCATTCGAGGGAGCCTCCGGGAGAGGAGCAACAATAGTCTT-3′
cdc25-S143A	5′-GTATTCCATTACCCAAGATGCCCCTCGAGTTTCCAGCACTATTGC-3′
cdc25-S143A GC	5′-GCAATAGTGCTGGAAACTCGAGGGGCATCTTGGGTAATGGAATAC-3′
cdc25-S308A	5′-CAAGCTGCACCCATTAAACCTATTGATATGTTACC-3′
cdc25-S308A GC	5′-GGTAACATATCAATAGGTTTAATGGGTGCAGCTTG-3′
cdc25-S332S334A	5′-CCTAGCTTGAAAGTTAGGGCGCCTGCTCCGATGGCATTCGC-3′
cdc25-S332S334A GC	5′-CCTAGCTTGAAAGTTAGGGCGCCTGCTCCGATGGCATTCGC-3′
cdc25-S332A	5′-TTGAAAGTTAGGGCCCCTTCTCCGATGA-3′
cdc25-S332A GC	5′-TCATCGGAGAAGGGGCCCTAACTTTCAA-3′
cdc25-S351A	5′-GATGAGCAAGATGCTCCAGTGCTTCGT-3′
cdc25-S351A GC	5′-ACGAAGCACTGGAGCATCTTGCTCATC-3′
cdc25-T379A	5′-GCCAAGATCTTGTGTGCGTGGCGCCAAAACAATCGACC-3′
cdc25-T379A GC	5-′GGTCGATTGTTTTGGCGCCACGCACACAAGATCTTGGC-3′